THE ASTROPHYSICAL JOURNAL, 546:886–897, 2001 January 10

FOUR YEARS OF EXTREME ULTRAVIOLET OBSERVATIONS OF MARKARIAN 421. II. TEMPORAL ANALYSIS

I. CAGNONI,[1,2] I. E. PAPADAKIS,[3] AND A. FRUSCIONE[2]
Received 2000 May 27; accepted 2000 July 31

ABSTRACT

The *Extreme Ultraviolet Explorer* (*EUVE*) satellite accumulated ~1,000,000 s of public data between 1994 and 1997 for the BL Lacertae object Markarian 421. This is the second of two papers in which we present the results of spectral and temporal analysis of this *EUVE* data set. We analyze in the present paper the imaging data by means of power spectrum and structure function techniques, while the spectral analysis is presented in a companion paper. We find for Mrk 421 a power spectrum with slope -2.14 ± 0.28 with a break at ~3 days. This is the first time that a break in the power spectrum of a BL Lacertae object has been found. We also find evidence of nonstationarity for Mrk 421 EUV emission.

Subject headings: BL Lacertae objects: individual (Markarian 421) — galaxies: active — galaxies: individual (Markarian 421) — galaxies: nuclei — ultraviolet: galaxies

1. INTRODUCTION

BL Lacertae objects are an extreme subclass of active galactic nuclei (AGNs) emitting highly variable nonthermal radiation over 20 decades of frequency from radio to TeV energies. The mechanism responsible for the production of radiation over such a wide range is thought to be synchrotron emission followed by inverse Compton scattering from energetic electrons. Some of the extreme properties of BL Lac objects, such as rapid variability, high gamma-ray luminosities, and superluminal motion (e.g., Urry & Padovani 1995), are explained invoking relativistic beaming of the emitted radiation along the jet axis, which is taken to be oriented at small angles to the line of sight.

Mrk 421 is one of the closest ($z = 0.0308$) and best-studied BL Lacertae objects. It is one of the strongest TeV sources and one of the brightest extragalactic EUV sources. The EUV emission of Mrk 421 during quiescence is believed to be the peak of a synchrotron spectrum. Mrk 421 was monitored by the *EUVE* satellite for 4 yr (1994, 1995, 1996, and 1998) as part of multiwavelength campaigns, and it was serendipitously observed in 1995 and in 1997 with the *EUVE* photometers for a total of 1,000,000 s, the best-sampled light curve for any BL Lac object at high energies.[4] Table 1 summarizes all the *EUVE* observations.

The main purpose of the present paper is to analyze in an homogeneous way the 1100 ks of *EUVE* public imaging data for Mrk 421 (less than half of it has been analyzed to date; Fruscione et al. 1996; Kartje et al. 1997) in order to perform the first detailed variability analysis (both in terms of power spectrum and structure function analysis) for a BL Lacertae object in the EUV. In general, variability studies by means of power spectrum analysis can reveal characteristic timescales of the emission mechanism (e.g., periodicities) and can constrain physical models. Our analysis reveals the existence of a characteristic timescale for Mrk 421 that can constrain current models.

The paper is organized as follows: All the *EUVE* light curves of Mrk 421 collected from 1994 to 1997 are presented in § 2. In §§ 3 and 4 we present the results from the power spectrum and structure function analysis, respectively. In § 5 we discuss those results. Finally in § 6 we make some concluding remarks. For the energy spectrum data and analysis, we refer the reader to the companion paper (Cagnoni & Fruscione 2000, hereafter Paper I).

2. OBSERVATIONS

A general description of the *Extreme Ultraviolet Explorer* satellite (*EUVE*) is given in Paper I. The photometric instruments on board *EUVE* are the Deep Survey/Spectrometer, (DS/S, covering the 68-178 Å band for photometry; Welsh et al. 1990) used for the deep EUV survey along the ecliptic and for pointed spectroscopic and imaging observations, and three co-aligned photometers (the "scanners"), observing in four different bandpasses (from 58 to 740 Å) and mounted orthogonally to the DS/S. The photometers were used to carry out the *EUVE* all-sky survey and are now employed in the Right Angle Program (i.e., the observation of serendipitous targets while the DS/S is conducting the primary science observation). Figure 1 shows a comparison of the DS/S and scanner effective areas.

Mrk 421 was observed several times from 1994 to 1997: four times with the DS/S and twice with the scanners; Table 1 summarizes these observations. Because of interstellar medium absorption along the line of sight ($N_H = 1.45 \times 10^{20}$ cm^{-2}; Elvis, Wilkes, & Lockman 1989), Mrk 421 was detected only in the Lexan/B filter (the shortest wavelength bandpass) both in the scanners (58-174 Å) and in the DS/S (67-178 Å).

2.1. *Serendipitous Sources*

Two faint serendipitous sources are clearly visible next to Mrk 421 in the DS image. We identified the closest one (~2′ from Mrk 421) with two unresolved stars in a double system: HD 95934 ($M_V = 6.00$, spectral type A3III-IV) and BD+39 2414B ($M_V = 12.6$). The other one at ~4′ from Mrk 421 was identified with another star in double system: HD 95976 ($M_V = 7.4$, spectral type FII).

The DS 50% energy radius is about 0.′3 up to 0.°3 off-axis. In scanner A, this half energy radius is ~3′ at ~1.°5–2° off-axis (where the sources lied in the 1995 and 1997

[1] SISSA, Via Beirut 4 -34138, Trieste, Italy; ilale@sissa.it.
[2] Harvard-Smithsonian Center for Astrophysics, 60 Garden Street, Cambridge, MA 02138.
[3] Physics Department, University of Crete, 710 03 Heraklion, Crete, Greece.
[4] As in Paper I, we are not considering the most recent observation (1998 April) since the data are presently being analyzed by the original proposers (Marshall et al., in preparation).

TABLE 1

EUVE OBSERVATIONS OF MRK 421

Year	Start	End	Instrument[a]	T_{exp}[b] (ks)	Count rate[c] (10^{-2} counts s^{-1})	Overall Variability Factor
1994.....	2 Apr	12 Apr[d]	DS	280	18 ± 0.085	2
1995.....	4 Feb	7 Feb	ScaA	68	32 ± 0.29	1.5
					45 ± 0.41	
1995.....	25 Apr	13 May	DS	355	29 ± 0.096	3
1995.....	25 Apr	28 Apr (flare)[e]			37 ± 0.23	
1995.....	29 Apr	6 May (decay)[e]			29 ± 0.15	
1995.....	7 May	13 May (quiescence)			22 ± 0.16	
1996.....	17 Apr	30 Apr	DS	299	30 ± 0.108	1.4
1996.....	10 May	11 May	DS	3.6	40 ± 0.11	
1997.....	7 Feb	11 Feb	ScaA	108	19 ± 0.16	2
					27 ± 0.22	

[a] "DS" indicates that the source was observed in the Deep Survey photometer. "ScaA" indicates that the source was observed in one of the three *EUVE* photometers (scanner A) during a pointing within the Right Angle Program.

[b] Total exposure time calculated eliminating (1) all SAA passages, (2) all satellite daytime data, (3) all times during which the detector was turned off, and (4) all times affected by possible earth blockage. It does include corrections for telescope vignetting, dead time and limited telemetry allocation (Primbshing).

[c] Average count rate in the Lexan/B filter ($\approx$60–180 Å). For the scanner observations, the second line gives the count rate normalized to the one in the DS assuming an average spectral shape, to take into account the difference in the effective area between the two instruments.

[d] This observation was presented in Fruscione et al. 1996.

[e] This observation was presented in Kartje et al. 1997.

observations) and the sources are not resolved. During the analysis of DS data we excluded a circle centered on HD 95934; this excluded only a negligible fraction of counts from Mrk 421.

2.2. *Light Curves*

We extracted the light curves from the DS or scanner time-ordered event lists using the *EUVE* Guest Observer Center software (IRAF/EUV package) and other IRAF timing tasks adapted for *EUVE* data. All the light curves were binned over one average *EUVE* orbit (5544 s), but effective exposure times per bin vary owing to several correction factors different case by case (e.g., instrumental dead time, telemetry saturation, high particle background, dead spot).

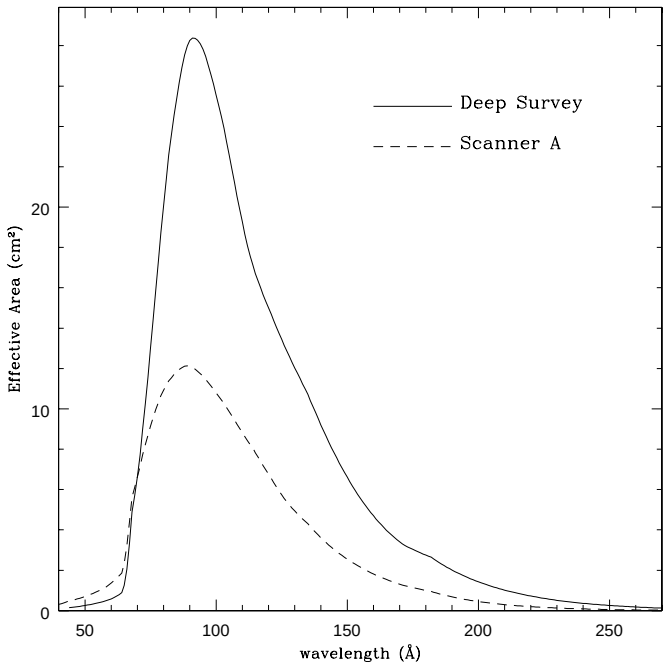

FIG. 1.—Comparison of the effective areas of the Deep Survey (*solid line*) and scanner A (*dashed line*) instruments on board the *EUVE* satellite.

Unless described otherwise, we chose the extraction region for the source as a circle with a 2.5 radius excluding a circle with a 0.67 radius centered on the serendipitous source. The background region is an annulus with inner and outer radii equal to $\sim 4'$ and $8'$, respectively, which avoids the other serendipitous source.

In order to compare scanner and DS data, we had to normalize the count rates. Count rates depend on the effective area of the telescope and on the spectral shape of the source. We convolved a sample of input spectra (absorbed power law with slopes as in Table 2 of Paper I) with the DS and scanner effective areas and defined the normalization factor as the ratio of peak of the derived count rates (see Fig. 2 as an example for $\alpha = 2$). The average normalization factor is about 1.4 ± 0.3 (depending on the input spectrum). We used this value throughout the paper and verified that the results in the power spectrum analysis are all consistent within the errors of this value.

The combined light curve of all the observations is presented in Figure 3. In this section we will give a qualitative description of each light curve in terms of flares and subflares: a general rising/decreasing trend will be addressed as a "flare," while faster variations superimposed on the general trend will be referred to as "subflares". This description is useful in understanding the results from the power spectrum and structure function analysis.

2.2.1. *1994 DS Light Curve*

Figure 4 shows the 1994 light curve, which was obtained eliminating time intervals when the source crossed the dead spot [5] (about 1440 s).

[5] A small region of reduced gain and detector quantum efficiency near the center of the DS detector, caused by the observation of the very bright EUV source HZ 43 (Sirk 1994).

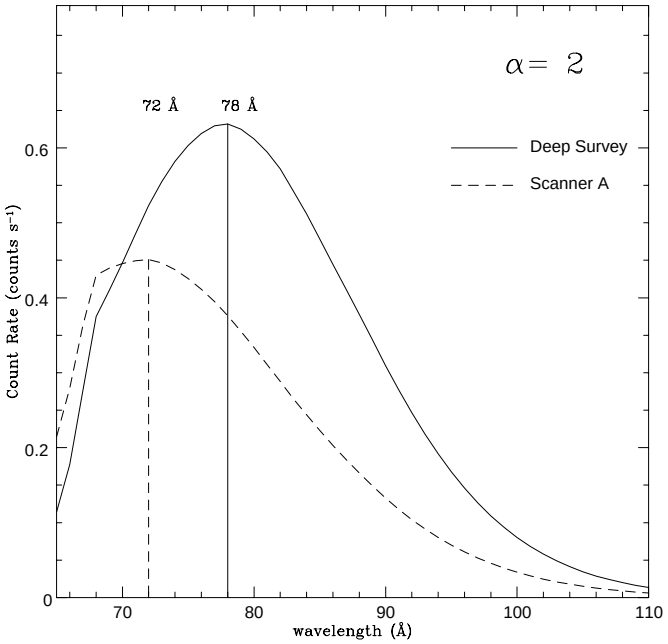

FIG. 2.—Simulated count rates in the DS (*solid line*) and scanner A (*dashed line*) instruments assuming an absorbed power-law model with spectral index $\alpha = 2$. The ratio of the count rate at the peak wavelength for the two instruments was used as rescaling factor to convert the scanner A count rate into a DS count rate.

The source dimmed for about 3 days, brightened again for another ~ 3.5 days, until it reached a level of ~ 0.2 counts s^{-1}, and stayed there for the remaining of the observation (another ~ 3.5 days). This light-curve behavior could be sampling the end of a flare and the beginning of a new one. Interestingly, when the source increases its flux, after MJD 49447, (i.e., possibly during the beginning of a new flare) smaller "subflares" are superimposed on it; this trend

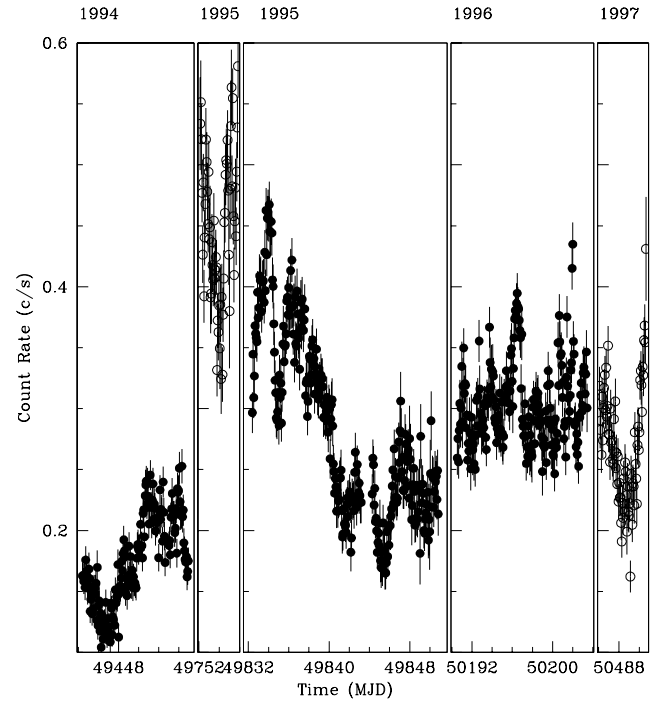

FIG. 3.—Combined light curve of all *EUVE* observations from 1994 to 1997 binned over one average *EUVE* orbit (~ 5544 s).

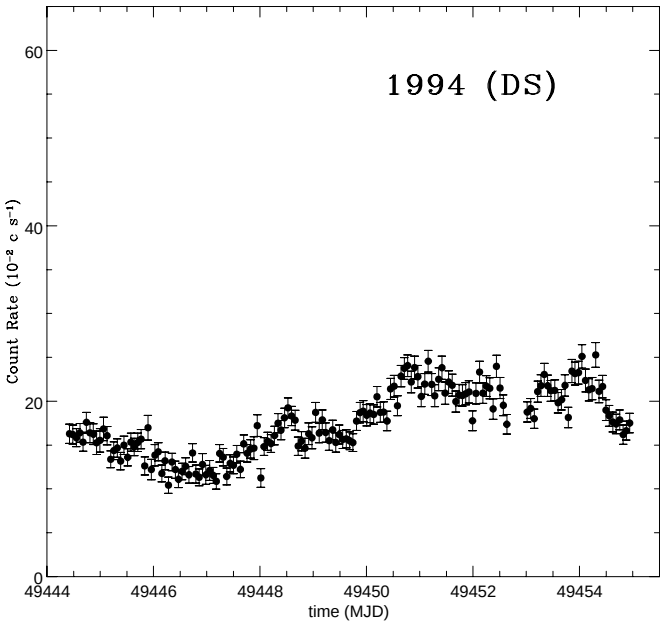

FIG. 4.—1994 April 2–12 Deep Survey light curve binned over one average *EUVE* orbit (~ 5544 s). This light curve was also presented in Fruscione et al. (1996).

is also present in the 1995 scanner light curve (see §2.2.2 and Fig. 5).

2.2.2. *1995 Scanner A Light Curve*

During this scanner exposure optimized for the primary scientific DS/S observation of HD 41511, Mrk 421 partially falls in the region usually discarded by the standard analysis pipeline because of the obscuration due to the filter support and because of the high particle background close to the detector edge. We extracted the light curve only from the "clean" region of the detector, and we corrected the count rate for the fraction of the count lost ($\sim 10\%$). The background region was chosen in the same detector quadrant as

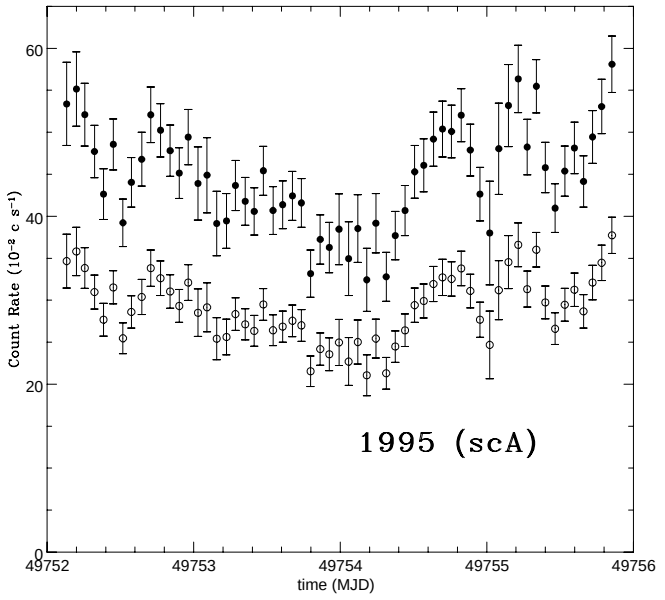

FIG. 5.—1995 February 4–7 scanner A light curve (*open circles*) binned over one average *EUVE* orbit (~ 5544 s). The filled circles represent the count rate scaled to the DS instrument (see § 2.2.2).

the source and large enough to match the ratio background/source (~ 7.8) region used for the other light curves. The light curve is plotted in Figure 5; the open circles represent the count rate measured in scanner A, while the filled circles are the count rate normalized to the DS; this light curve has as behavior similar to the 1994 DS light curve: when the source brightens, after MJD 49754, "subflares" appear above the main trend.

2.2.3. *1995 DS Light Curve*

During this DS/S observation, the source was pointed 0°.3 off axis both to avoid the dead spot and to extend the spectrum toward shorter wavelengths (see Paper I). The light curve is shown in Figure 6.

The behavior of the source during the DS 1995 observation is complex: at the beginning Mrk 421 brightens by a factor of $\sim 65\%$ in less than 2 days, and this flare, which lasts for about 3 days, is well correlated to a TeV/X-Ray flare (Buckley et al. 1996). Right after the first one, there is a second flare lasting for ~ 6 days, which can also be seen as the superposition of two separate flares (the second one starting at $\sim$ MJD 49838). After MJD 49845.5, the source rises from ~ 0.20 counts s^{-1}, up to ~ 0.28 counts s^{-1}, and then decays to ~ 0.23 counts s^{-1}, within ~ 3 days. The overall variability of the source is about a factor 3.

2.2.4. *1996 DS Light Curves*

In 1996 Mrk 421 was observed few days before and few days after the detection of a large TeV flare on 1996 May 7 (Zweerink et al. 1997). The light curves are shown in Figure 7. This light curve looks different from all the other ones because no slow variations seem to be present; the source appears to be at a constant level with lots of small amplitude, fast variations superimposed on it; i.e., the light curve appears to be the sum of flares which live a short time, and rise or decay faster when compared with the flares seen in the other light curves (see for example the two flare like events after MJD = 50200).

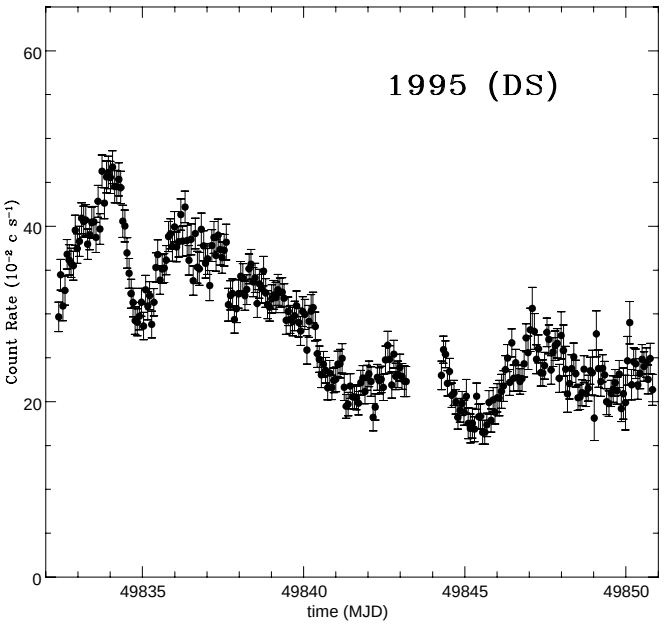

FIG. 6.—Same as Fig. 4, but for the 1995 April 25–May 13 DS data. The data from MJD 49832 to MJD 49843 were presented in Kartje et al. (1997) and were part of a multiwavelength campaign during which a TeV flare was detected (Buckley et al. 1996).

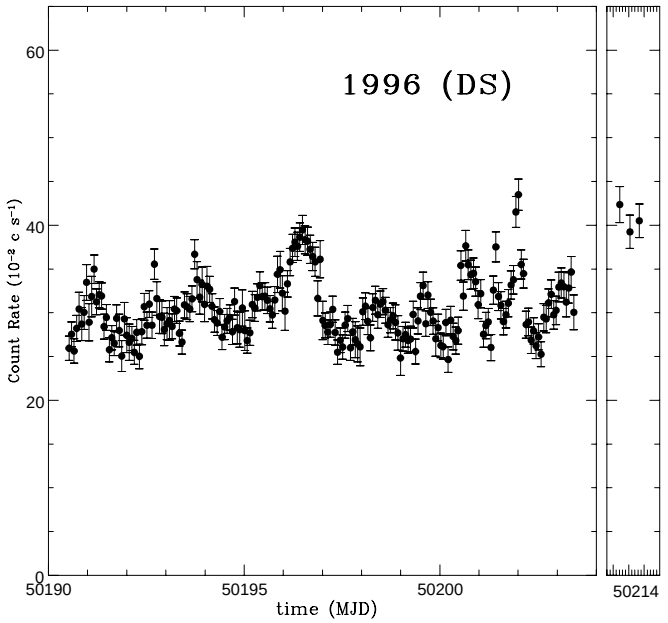

FIG. 7.—Same as Fig. 4, but for the April 17–30 DS data (*left*) and the May 10-11 data (*right*). A large TeV flare (Zweerink et al. 1997) occurred on 1996 May 7.

2.2.5. *1997 Scanner A Light Curve*

In 1997 Mrk 421 was observed for 4 days with the scanner A telescope during the DS pointed observation of Γ Tauri; the source was detected within the useful area of the scanner A field of view, allowing an easier data reduction than the previous scanner observation. The light curve is shown in Figure 8: the open circles represent the scanner data while the filled circles correspond to the count rate normalized to the DS. This is the shortest light curve, and its shape suggests that we may be looking at the tail of a flare and at the beginning of a new one.

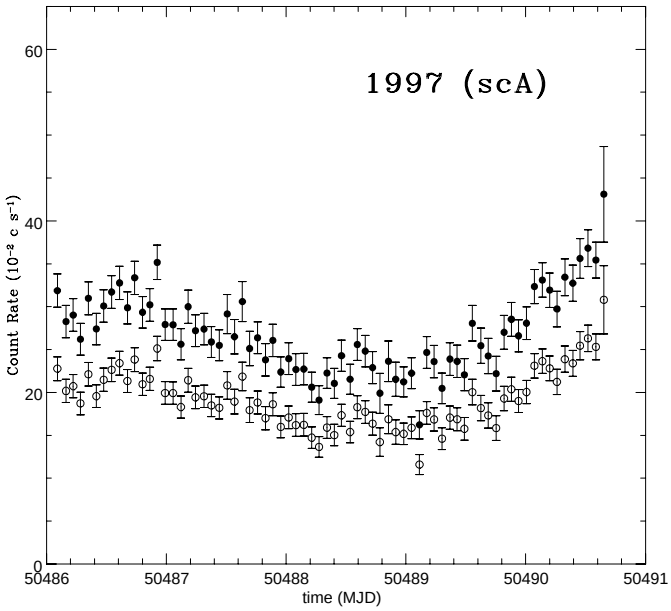

FIG. 8.—Same as Fig. 5, but for the 1997 February 7–11 1997 scanner A data.

3. POWER SPECTRUM ANALYSIS

In order to quantify the variability seen in the *EUVE* light curves of Mrk 421, we computed their periodogram as

$$\hat{I}(\nu_i) = \frac{\Delta t}{N}\left\{\sum_{i=1}^{N}[x(t_i) - \bar{x}]e^{-i2\pi\nu_i t_i}\right\}^2 - C\,, \qquad (1)$$

where $\bar{x}$, Δt, and N are the mean value, bin size, and number points of each light curve, respectively, and $\nu_i = i/(N\Delta t)$, $i = 1, 2, \ldots, (N/2) - 1$ (e.g., Deeming 1975). The constant C in equation (1) represents the power level due to Poisson statistics, $C = \Delta t\sigma^2_{\rm noise} = (\Delta t/N)\sum_{i=1}^{N} {\rm err}(i)^2$ [err(i) is the error of each light curve point]. The subtraction of this constant level is necessary since we are interested in the source power spectrum only and the *EUVE* light curves were obtained with two different instruments; hence the Poisson statistics will be different in them. The periodogram calculated in this way has the units of (counts $s^{-1})^2$/Hz, and its integral over positive frequencies is equal to half the light-curve variance.

It is common to average the periodogram estimates in order to reduce the variance and approximate their probability distribution function to a Gaussian. Furthermore, it is better to estimate the logarithm of the power spectrum instead of the power spectrum itself, since the logarithmic transformation brings the distribution function of the power spectrum estimates closer to a Gaussian (Papadakis & Lawrence 1993). Therefore, we calculated the logarithm of the binned periodogram estimates,

$$\log_{10}[\hat{P}(\nu_i)] = \log_{10}\left[\frac{\sum_j \hat{I}(\nu_j)}{m}\right], \qquad (2)$$

where $\nu_i = \sum_j \nu_j/m$, and $\nu_j = j/(N\Delta t)$, and used it as our estimate of the *logarithm* of the power spectrum. The index j varies over m consecutive periodogram estimates, and the index i varies over the $[(N/2) - 1]/m$ subsets into which we have grouped the periodogram estimates. Taking into account the propagation of errors (e.g., Bevington 1969), the error on the logarithm of the power spectrum is

$$\sigma\{\log_{10}[\hat{P}(\nu_i)]\} = \log_{10}(e)\sigma_{\hat{P}(\nu_i)}/\hat{P}(\nu_i)\,, \qquad (3)$$

where $\sigma_{\hat{P}(\nu_i)}$ is the square root of the variance of the value of $\hat{I}(\nu_j)$ around the mean value, $\hat{P}(\nu_i)$, at each bin.

3.1. *Power Spectra of the Orbit-binned Light Curves*

We estimated the power spectrum of the DS and scanner A light curves binned over one average *EUVE* orbit (5544 s) shown in Figures 3–8. To avoid the gap in 1995 DS observation (Fig. 6) we divided it into two parts and performed a power spectrum analysis on each one of them. Using equations (1) and (2), we estimated the logarithm of the power spectrum with $m = 10$. A larger value for m would bring the distribution function of the power spectrum estimates closer to a Gaussian (Papadakis & Lawrence 1993). However, this small value of m was necessary in order to have a reasonable frequency resolution, i.e., in order to have the maximum possible number of power spectral points above the Poisson noise level.

The power spectra of all the light curves, normalized to the square mean value of the respective light curve, are shown in Figure 9. The normalization is necessary if one wants to compare the power spectrum amplitudes, since the light curves were obtained from two different instruments. All the power spectra show a similar red noise behavior at frequencies less than $10^{-4.3}$ Hz (i.e., all of them rise logarithmically toward lower frequencies in a similar way), except for DS 1996 observation which seems to flatten for $\nu < 10^{-5}$ Hz.

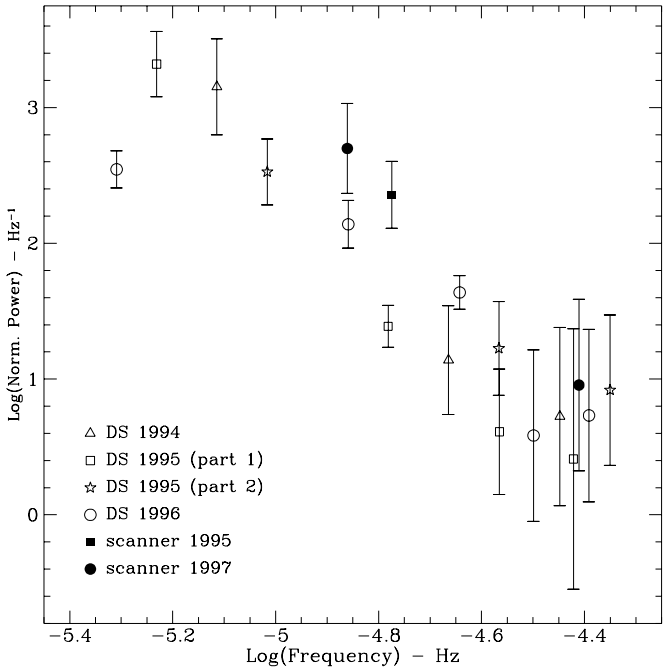

FIG. 9.—Normalized power spectrum (binning factor $m = 10$, see § 3.1) obtained from each light curve binned over 5544 s (1 average *EUVE* orbit). 1995 DS/S observation was split into two parts to avoid the gap. The open symbols represent DS/S observations (*triangles for 1994, squares for the first part of 1995, stars for the second part of 1995, and circles for 1996*), while the filled symbols represent scanner observations (*squares for 1995 and circles for 1997*).

We fitted the DS power spectra with a simple power-law model of the form $P(\nu) = A \times (10^{-5}\nu)^{-\alpha}$ (the scanner A power spectra had too few points to fit a model to them). In this model, the normalization A is equal to the value of $P(\nu)$ at $\nu = 10^{-5}$ Hz. The model fit was done using the power spectra before normalizing to the mean square value. The best model fit results are listed in Table 2. The model gives a good fit to all the DS power spectra, but, owing to the small number of points, the errors on the model parameters are large. The best-fit values of A are within the errors for all the DS spectra. However, the best-fit slope values show a larger scatter. In particular, the difference between the DS 1995 (part 1) and the DS 1996 best-fit slope values is 2.7 ± 1.0. This $\sim 3\,\sigma$ difference indicates that the shape of the power spectrum does not remain constant with time, i.e., that the EUV emission of Mrk 421 is not stationary.[6] However, looking at DS 1996 power spectrum (Fig. 9), there is a possibility that the flatter slope obtained from the fit is due to a flattening around $\nu = 10^{-5}$ Hz. If this is the case, a broken power-law model should give a better fit to the data. However, with just 5 points, it is not possible to investigate if a broken power improves the fit to the data in a statistically significant way (e.g., by the use of an F-test). On the other hand, perhaps the flattening of the power spectrum is a spurious effect introduced by the small binning

[6] A light curve is said to be stationary if its mean, variance, and power spectrum remain constant in time (e.g., Chatfield 1989); see § 5.4 for further details.

TABLE 2

POWER SPECTRA "POWER-LAW" MODEL FITS FOR THE DS ORBIT-BINNED LIGHT CURVES OF MRK 421

Year	Instrument	α	A	No. of Points	χ^2
1994	DS	4.02 ± 1.42	13 ± 24[a]	3	0.38
1995 (part 1).....	DS	4.14 ± 0.86	22 ± 15[a]	4	0.35
1995 (part 2).....	DS	2.64 ± 1.10	15 ± 8[a]	3	0.17
1996	DS	1.45 ± 0.42	13 ± 6[a]	5	3.85
All	DS+ScaA	2.14 ± 0.28	148 ± 33[b]	10	5.6

[a] In units of $(\text{counts s}^{-1})^2/\text{Hz}$

[b] In units of Hz^{-1}

used ($m = 10$). In an attempt of ruling out this possibility we used a larger value ($m = 20$). Figure 10 compares the results: open circles for $m = 10$ (as in Fig. 9) and filled circles for $m = 20$. Both power spectra look similar, and the lack of frequency resolution in the latter case cannot allow us to reach a firm conclusion.

Despite this possible nonstationarity, it is useful to combine the periodograms of all the DS and scanner A light curves in order to increase the number of power spectrum estimates (and hence the frequency resolution). We first normalized the data sets to the square mean value of the respective light curve and then combined them into one data set by sorting them in order of increasing frequency. Then we grouped this "combined" periodogram into bins of size $m = 20$ since the larger number of estimates allows us to use a larger bin size value. Figure 11 shows a plot of the resulting power spectrum (*filled circles*). Note that the combined power spectrum has the units of Hz^{-1}. This spectrum can be considered as the "average" *EUVE* power spectrum of the source. A power-law model gives a good fit to this average power spectrum (solid line in Figure 11; Table 2) with a best-fit slope value of 2.14 ± 0.28.

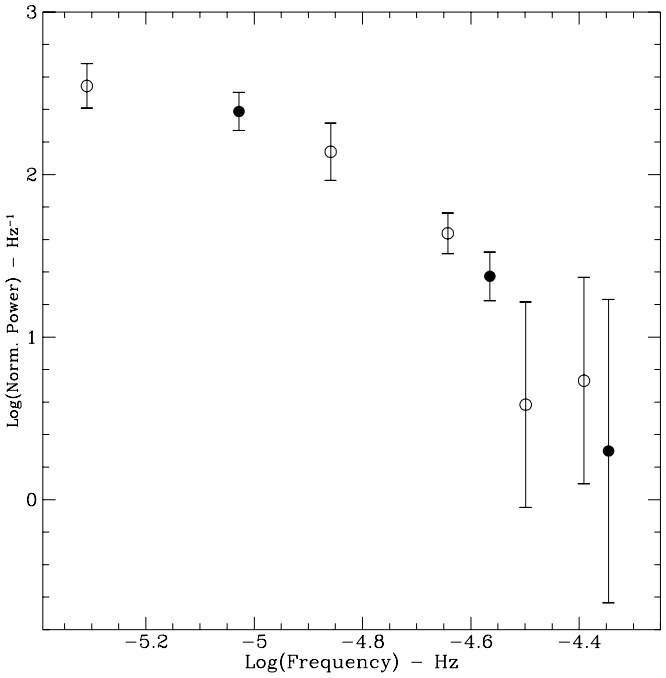

FIG. 10.—Same as Fig. 9, but for DS 1996 observation with different binnings. Opens circles, as in Fig. 9, represent a binning value of $m = 10$, and filled circles represent a binning value of $m = 20$ (see § 3.1).

3.2. *Power Spectra of the 500 s Binned Light Curves*

Because of the indication of a possible break in the power spectrum and/or a possible nonstationarity in the *EUVE* light curve of Mrk 421, we decided to investigate further the power spectra of the DS 1995 and 1996 light curves. Our main aim was to determine the low-frequency shape of the power spectrum as well as possible. For this reason, we used a ~ 10 times finer binning, with a bin size of 500 s, for the light curves; we were thus able to extend the power spectrum to lower frequencies and to use a larger value for m ($m = 20$ in eq. [2]) to bring the distribution function of the power spectrum estimates closer to a Gaussian.

Figure 12 shows the DS 1995 and 1996 power spectra estimated with equation (1), without subtracting the expected Poisson noise level, and binned as in equation (2) with $m = 20$; the long-dashed lines in these plots indicate the Poisson noise power level C. Both power spectra show a large peak at $\sim 1.8 \times 10^{-4}$ Hz corresponding to a period of 5556 s, i.e., the *EUVE* orbital period. The next strongest peak is at a harmonic of that frequency. These peaks are due to the uneven sampling of the 500 s binned light curves.

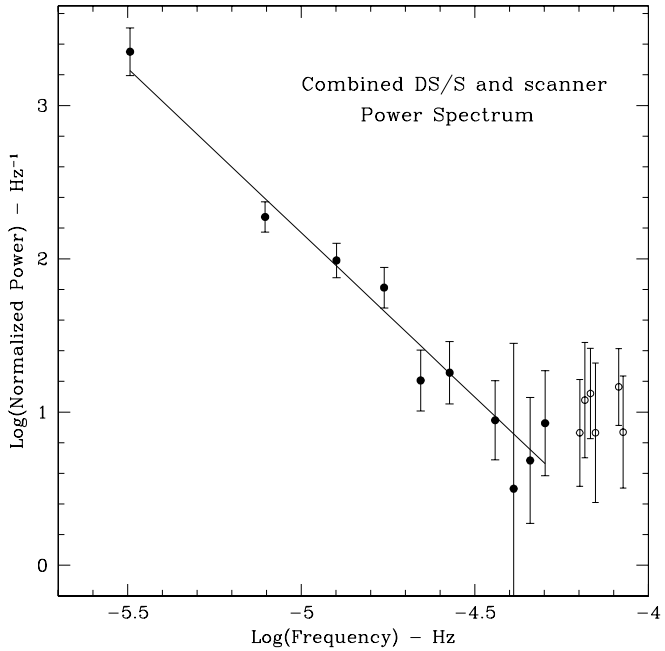

FIG. 11.—Average normalized power spectrum of Mrk 421 obtained from all the 5544 s binned light curves presented in Fig. 3 (see § 3.1). Different symbols represent different binnings: $m = 20$ (*filled circles*) for the low-frequency part and $m = 10$ (*open circles*) for the high-frequency part representing the Poisson noise level. The solid line shows the best power-law model fit with slope -2.14.

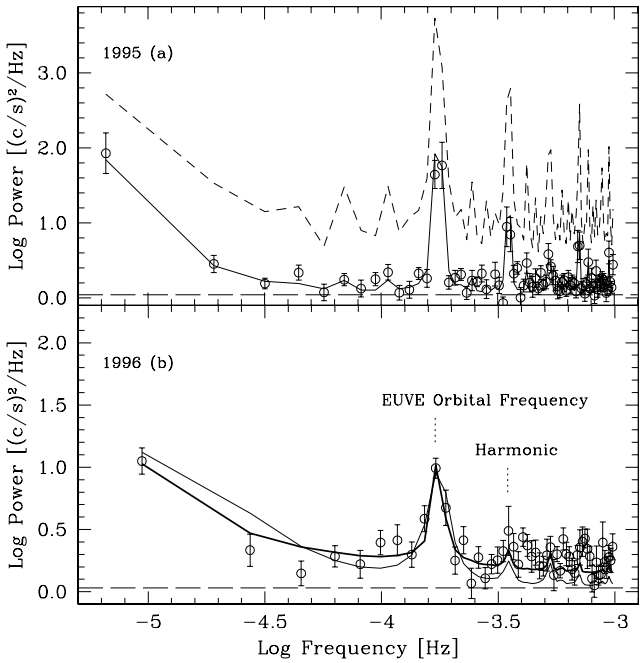

FIG. 12.—Power spectra of the DS 1995 (*a*) and DS 1996 (*b*) light curves binned over 500 s (*open circles*). The long-dashed line in both plots indicate the expected Poisson noise power level. The solid line shows the best fit of the model defined by eq. (5) in § 3.2, with the slope fixed to −2.14. The dotted line in (*a*) represents the simulated power spectrum using the same best-fit values but moving the break to 10^{-7} Hz, while the thick line in (*b*) shows the best fit of the same model but with the slope left as a free variable (see text).

Apart from those peaks, the two power spectra appear to have a similar shape: they rise toward low frequencies, and they are flat at higher frequencies. So, it seems as if the use of a smaller bin size in the light curves has not helped us much. The power spectra, at most frequencies, appear to be flat and dominated by the Poisson noise power. However, while the DS 1995 estimates at high frequencies are close to the expected Poisson power level, the DS 1996 power spectrum is higher than this level.

We fitted both spectra with a modified power-law model with one of the slopes fixed at 2.14 (see below). Owing to the effects of the window function, it is not possible to fit the logarithm of the model directly to the power spectrum calculated from the 500 s binned light curves. Instead, we convolved the model, let us say $M(v)$, with the window function at each frequency v_i,

$$I_{mdl}(v_i) = \frac{\Delta t}{N} \int_{-\infty}^{+\infty} M(v) W(v_i - v) dv \ . \qquad (4)$$

The function $I_{mdl}(v_i)$ takes account of the window function effects. We call $I_{mdl}(v_i)$ the "convolved model."

As $M(v)$, we used the following function,

$$M(v) = \frac{A}{[(2\pi v)^2 + f_b^2]^{\alpha}} + C \ , \qquad (5)$$

which has a power-law form with a slope of 2α at frequencies $\gg f_b/2\pi$, and flattens to zero slope at frequencies $\ll f_b/2\pi$ (as before, C represents the power level due to the Poisson counting statistics). Note that as $M(v)$ we did not use a simple power-law model because in this case it is not easy to estimate the convolution model (eq. [4]) analytically (a simple power-law model cannot be defined at $v = 0$) and because there might indeed be a break, as suggested by the DS 1996 power spectrum (Fig. 9).

Then we averaged the convolved model $I_{mdl}(v_p)$ over groups of size $m = 20$ exactly as we did when estimating the power spectrum. The logarithm of the convolved model power spectrum becomes

$$\log_{10} [P_{mdl}(v_i)] = \log_{10} \left[\frac{\sum_j I_{mdl}(v_j)}{m} \right] . \qquad (6)$$

We can now fit $\log_{10} [P_{mdl}(v_i)]$ to the estimated power spectrum, $\log_{10} [\hat{P}(v_i)]$. In this way, we are taking into account both the window function and any effect that the binning procedure may have on the power spectrum estimate.

For the fit we used standard χ^2 statistics, we kept 2α fixed to the value 2.14, and we did not allow C to vary but rather used the value found as described at the beginning of § 3. Table 3 summarizes the best-fit results for each observation; the errors quoted represent the 90% confidence levels assuming that A and f_b are correlated. By far the largest χ^2 value is for the DS 1996 model fit. However, it is not straightforward to judge the goodness of fit using the these χ^2 values. Because of the uneven sampling of the light curves, the periodogram estimates are no longer independent. Therefore, the errors on $\log_{10} [\hat{P}(v_i)]$ may be larger than those estimated (and hence the χ^2 values smaller). At the same time, depending on the amount of correlation between the $\hat{I}(v_i)$'s, the $\log_{10} [\hat{P}(v_i)]$ estimates may be correlated as well. As a result, the number of degrees of freedom may be smaller than those listed in Table 3.

The best model fits are also plotted in Figure 12 with a solid line; these plots show that the model agrees well with the DS 1995 power spectrum, but not with the DS 1996 (as expected from the large χ^2 value). We fitted again the DS 1996 power spectrum with the model defined in equation (5), but we left the slope as a free parameter this time. The best-fit results are listed in Table 3 (values in a parenthesis),

TABLE 3

POWER SPECTRA —"POWER-LAW PLUS LOW-FREQUENCY TURNOVER" MODEL FIT FOR THE DS AND SCANNER A, 500 s BINNED LIGHT CURVES OF MRK 421

Year	Instrument	Slope 2α	f_b (Hz)	Degree of Freedom	χ^2
1994.....	DS	2.14 (fixed)	$8.4^{+27}_{-7.7} \times 10^{-6}$	43	67.8
1995.....	ScaA	2.14 (fixed)	$5.0^{+18}_{-4.3} \times 10^{-5}$	14	28.7
1995.....	DS	2.14 (fixed)	$2.6^{+5.6}_{-2.0} \times 10^{-6}$	77	116.9
1996.....	DS	2.14 (fixed)	$7.7^{+4.3}_{-2.6} \times 10^{-5}$	53	140.4
		(1.1 ± 0.1)	$(1.6^{+10.}_{-1.5} \times 10^{-6})$	(52)	(65.5)
1997.....	ScaA	2.14 (fixed)	$7.7^{+17}_{-5.3} \times 10^{-5}$	17	16.7

and the best-fit model is also plotted in Figure 12*b* (*thick line*). As this figure shows, the new model fit agrees better with the power spectrum. The best-fit slope is now 1.1 ± 0.1, significantly smaller than the average slope of 2.14 ± 0.28. The χ^2 value is also reduced by 74.9. The ratio of the reduced χ^2 values for the two fits is 2.1 (note that this ratio does not depend on whether the errors on the power spectrum are underestimated or not). Using the number of degrees of freedom listed in Table 3 and the *F*-test, we find that the improvement on the fit when we let the slope to be a free variable is highly significant (the probability of a significantly better fit when $\alpha = 1.1$ is larger than 99.5%). The probability remains larger than 95%, even if the degree of freedoms listed in Table 3 are reduced by a factor of 2.

Furthermore, to check for any other possible indication of nonstationarity, we performed a fit to the power spectra of all the 500 s binned light curves (including the scanner A light curves) using the model defined in equation (5) with $2\alpha = 2.14$. The best-fit model results are listed in Table 3, and the best-fit model, together with the power spectra, are plotted in Figure 13 (*the dashed lines in this figure show the Poisson noise power level*). This figure shows that the model gives a good fit to all the power spectra.

We conclude that all the *EUVE* power spectra of Mrk 421 are consistent with a power-law model with a slope of ~ 2.1. The only exception is the power spectrum of the DS 1996, which shows a significantly flatter slope of 1.1 ± 0.1. The clear change in slope in the 1996 data shows that the EUV emission of Mrk 421 is not statistically stationary (see § 5.4).

As hinted by Figure 9 for DS 1996 (*open circles*), from the fit of the 500 s binned power spectra we found indication for the presence of a low-frequency turnover in the *EUVE* power spectrum of Mrk 421 below which the power spectrum flattens. This finding, if confirmed, would be the first detection of a break in the power spectrum of a BL Lac object. Since we cannot estimate the power spectrum at frequencies lower than $\sim 10^{-5}$ Hz, using the value $m = 20$, we cannot be certain of the slope below the turnover frequency. All we can say with the present data is that the power spectrum should show a change in its slope at f_b. Furthermore the value of this knee frequency is not constrained very well from our data. Using the best-fit results from the DS spectra only (as they have the largest number of data points), we get a straight mean value of $f_b = 4 \times 10^{-6}$ Hz. By simply combining the overlapping 90% confidence limits on the best values of f_b, we find that with probability larger than 68%, f_b should be between 7×10^{-7} Hz and 8×10^{-6} Hz.

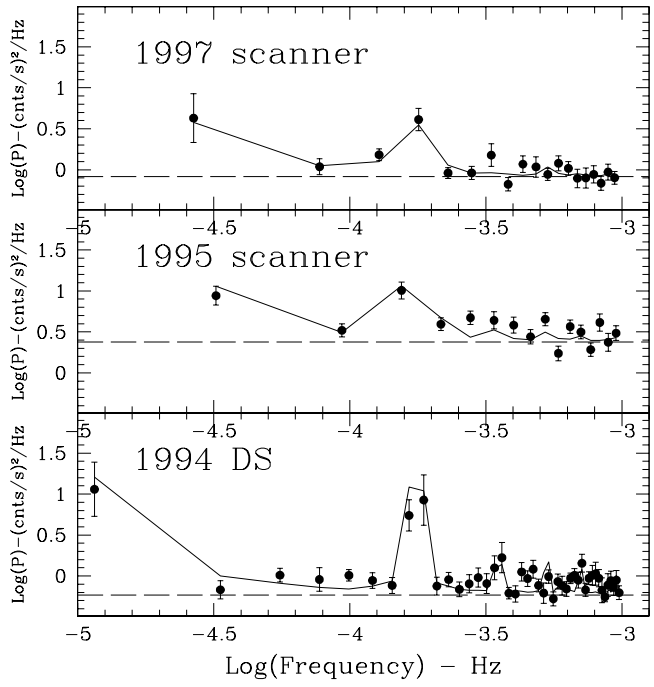

FIG. 13.—Same as Fig. 12, but for DS 1994, scanner A 1995 and scanner A 1997, respectively.

From a physical point of view, it is natural to expect that low-frequency knees should be present in the power spectra of AGNs. Lack of this turnover would imply a physical system with infinite variance, a system whose properties change continuously with time. The frequency turnover is not evident in the combined *EUVE* power spectrum of Mrk 421 (Fig. 11), because that spectrum does not extend to frequencies below $\sim 10^{-5.5}$ Hz. Its presence is implied only when we take proper account of the window function effects in the model fitting of the 500 s light-curve power spectra. If the frequency turnover were located at a much lower frequency, more power would be transferred to higher frequencies. The resulting power spectrum would have a higher normalization than the observed one. To put it in other words, the amplitude of the variations in the light curves would be larger, i.e., they should have a higher variance. For example, let us assume that the source power spectrum is well described by equation (5) and that the break is at 10^{-7} Hz. Using equations (4) and (6) we can predict how the power spectrum of the DS 1995 light curve should be in this case (dashed line in Fig. 12*a*). As this figure shows, the power spectrum should have a much larger amplitude than the one that is actually observed.

Owing to the significance of such a feature in the power spectrum of the source, we searched further evidence of its existence by means of a structure analysis of the light curves. We present below the results from this analysis of the *EUVE* light curves that confirm the existence of this turnover in the power spectrum of Mrk 421.

4. STRUCTURE FUNCTION ANALYSIS

The structure function (SF hereafter) is defined as

$$\mathrm{SF}(\tau) = 2\sigma^2 - R(\tau)\,, \tag{7}$$

where σ and $R(\tau)$ are the variance and auto-covariance at lag τ of the light curve (eq. [A4] in Simonetti, Cordes, & Heeschen 1985). For a given light curve, it is usually estimated by

$$\widehat{\mathrm{SF}}(\tau) = \frac{1}{N}\sum_{i=1}^{N-\tau}[x(i+\tau) - x(i)]^2\,, \tag{8}$$

(eq. [A8] in Simonetti et al. 1985). The SF gives a measure of the mean difference in the flux of two light-curve points, as a function of their time separation (lag) τ. There is a simple correspondence between the SF and the power spectrum: when $P(\nu) \propto \nu^{-\alpha}$, then $\mathrm{SF}(\tau) \propto \tau^{\alpha-1}$. Furthermore, if the power spectrum flattens below a frequency f_b, then $\mathrm{SF}(\tau) \sim 2\sigma^2$ in the limit $\tau \gg 1/f_b$.

The main advantage of the structure function analysis is that the SF estimation is not affected by gaps of missing points in the light curve (it is easy to show using eq. [8], that $\langle \widehat{\mathrm{SF}}(\tau) \rangle = \mathrm{SF}(\tau)$, irrespective of the light-curve sampling pattern). However, it is difficult to estimate the errors on $\widehat{\mathrm{SF}}(\tau)$ because, as with estimates of other time domain quantities (e.g., auto- and cross-correlations), the SF estimates at different lags are heavily correlated (much more so than the periodogram points at different frequencies, even in the case of unevenly sampled data).

To estimate the SF of Mrk 421, we used together all the orbit-binned DS and scanner A light curves and constructed a single, long *EUVE* light curve of the source (in order to use the scanner data into an overall light curve, we normalized them to the DS expected count rate as explained in § 2.2). For each pair of data points in the light curve, $x(t_i)$ and $x(t_j)$, we computed their time difference, $\Delta t_{i,j} = t_i - t_j$, and their flux difference, $\mathrm{FD}_{i,j} = x(t_i) - x(t_j)$. Let us assume that we have chosen a lag bin of size $\Delta\tau$, and that there are n points with $\Delta t_{i,j}$ in the interval $[\tau - \Delta\tau/2, \tau + \Delta\tau/2]$. We used the average value of the n $\mathrm{FD}_{I,J}$ measurements, $\sum \mathrm{FD}_{i,j}/n$, as an estimate of the structure function, $\widehat{\mathrm{SF}}(\tau')$, at the lag $\tau' = \sum \Delta t_{i,j}/n$.

For the overall *EUVE* light curve (Fig. 3), we estimated the SF twice. The first time we used $\Delta\tau = 1$ day, and the second time $\Delta\tau = 1$ month. The first bin value was used to estimate the SF from lag $\sim$1 day up to lag $\sim$18 days. We cannot estimate the SF at higher lags with $\Delta\tau = 1$ day since the individual *EUVE* light curves of Mrk 421 have a maximum length of $\sim$20 days. Consequently, we used the larger bin size ($\Delta\tau = 1$ month) to estimate the SF at lags more than 2 months and up to $\sim$2.5 yr (i.e., the time interval between the first and last *EUVE* light curve of Mrk 421).

The combined short and long bin estimated SF is plotted in Figure 14 (*filled circles for* $\Delta\tau = 1$ *day and filled squares for* $\Delta\tau = 1$ *month*). The estimated SF rises roughly logarithmically with τ at lags less than 20 days. However, at lags more than 60 days it is relatively flat. This flattening cannot be due to the uneven sampling of the light curve, but it is exactly what we would expect if there is a low-frequency turnover in the power spectrum of Mrk 421.

We examine below whether the estimated SF shown in Figure 14 is consistent with the assumption that the true power spectrum of Mrk 421 is similar to the model defined by equation (5) with $2\alpha = 2.14$ and $f_b = 4 \times 10^{-6}$ Hz.

To answer this question, we performed a numerical experiment: we created one set of 1000 simulated light curves using the method described in Appendix C of Papadakis & Lawrence (1995). Each simulated light curve has a power spectrum with slope of 2.14, a knee frequency at 4×10^{-6} Hz, and variance as the *EUVE* light curve. For each one of the simulated light curves, we estimated the SF exactly in the same way as we did with the *EUVE* light curve. Then we computed the expected mean value, $\langle \mathrm{SF}_{\mathrm{sim}} \rangle$, and variance, $\sigma^2_{\langle \mathrm{SF}_{\mathrm{SIM}} \rangle}(\tau)$, of all the simulated SFs at each τ. The results are plotted in Figure 14 (*open circles and open squares for the mean short- and long-bin simulated SF*). The "errors" on the points are equal to $\pm\sigma_{\langle \mathrm{SF}_{\mathrm{sim}} \rangle}(\tau)$. Note

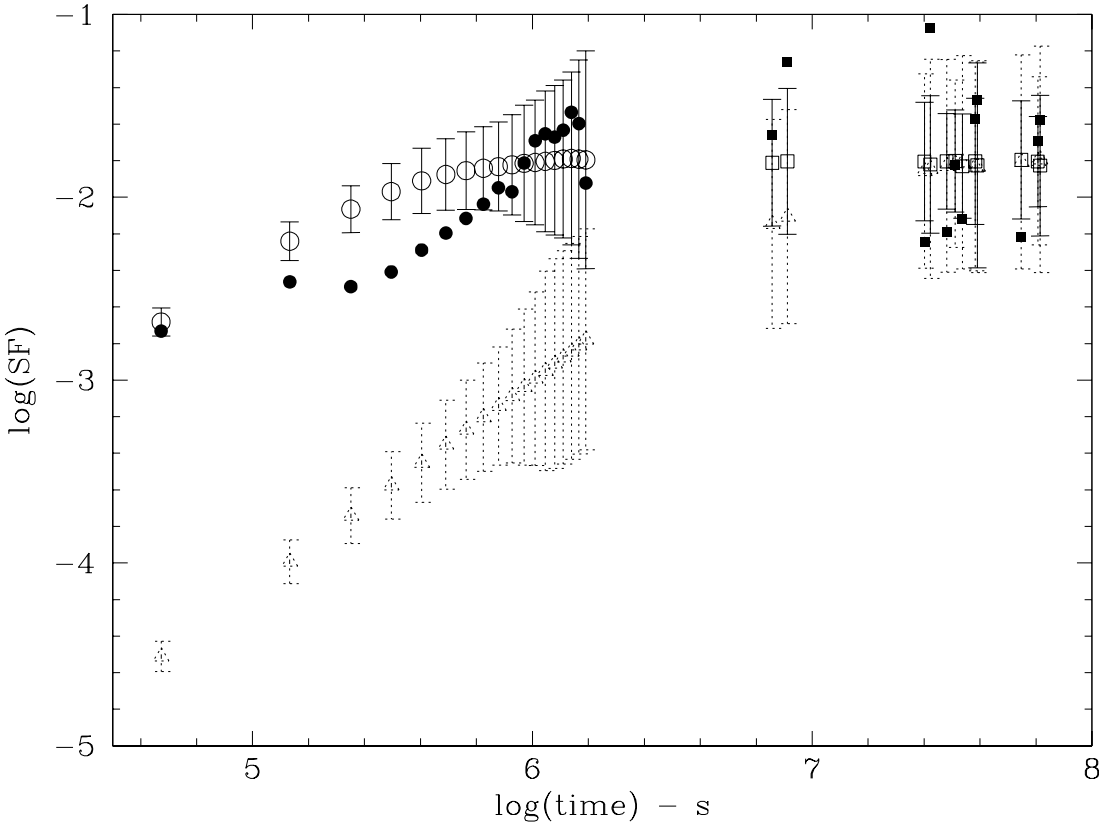

FIG. 14.—Structure function of the total *EUVE* light curve of Mrk 421 (Fig. 3). Filled circles correspond to the SF estimated with a lag bin of size 1 day and the filled squares to the SF estimated with a lag bin of size 1 month. Open symbols (*circles* and *squares*) correspond to the mean SF of 1000 simulated light curves with a power spectrum of slope 2.14 and a frequency turnover at 4×10^{-6} Hz. Dotted triangles correspond to the mean SF of 1000 simulated light curves with a same slope power spectrum, but with a frequency turnover at 10^{-7} Hz. In both cases, the error bars correspond to the standard deviation of the simulated SFs around their mean (see § 4 for details).

that these errors would represent the 68% of the process realizations in the case of a Gaussian distribution, but, since the actual SF are *not* normally distributed, they can only give us an idea of the real 1 σ errors of the actual SF and cannot be used in the normal χ^2 estimation. In order to quantify the comparison between $\log [\langle \mathrm{SF}_{\mathrm{sim}}(\tau) \rangle]$ and $\log [\hat{\mathrm{SF}}(\tau)]$ in a statistical way, we estimated the sum of their squared differences, i.e., $\sum_i \{\log [\langle \mathrm{SF}_{\mathrm{sim}}(\tau_i) \rangle] - \log [\hat{\mathrm{SF}}(\tau_i)]\}^2$, for all the τ_i for which we have estimated the SF. We refer to this sum as "χ^2," although its definition is different from the traditional definition of χ^2. In our case, $\chi^2 = 4$. Based on the distribution of the χ^2 values for the 1000 simulated light curves, the probability that the *EUVE* light curve of Mrk 421 is a realization of a process with a power spectrum with a knee frequency at 4×10^{-6} Hz is $\sim 40\%$.

Finally to check whether Mrk 421 structure function is consistent with a break at timescales longer than the range suggested by the fit of the power spectra, we performed a second numerical experiment: we created a new set of 1000 simulated light curves, with $2\alpha = 2.14$, variance as the *EUVE* light-curve variance, and a knee frequency at 10^{-7} Hz. As above, for each simulated light curve we estimated the SF, and then computed $\langle \mathrm{SF}_{\mathrm{sim}}(\tau) \rangle$, and $\sigma_{\langle \mathrm{SF}_{\mathrm{sim}} \rangle}(\tau)$. The results for the mean short-and long-bin simulated SF are plotted in Figure 14 (*dotted triangles*). At large lag values the mean simulated SF agrees well with the SF of Mrk 421. This is not surprising since, as we mentioned at the beginning of this section, we expect that SF $\sim 2\sigma^2$ in the limit when τ is larger than $1/f_b$ (10^7 s in this case). However, the agreement between the mean simulated SF and the Mrk 421 SF at short lags is not good. The χ^2 this time is equal to 183. Based on the distribution of the χ^2 values for the 1000 simulated light curves, the probability that the *EUVE* light curve of the Mrk 421 is a realization of a process with a power spectrum with a knee frequency at 10^{-7} Hz is less than 0.1%.

We conclude that the SF of Mrk 421 (Fig. 14) is entirely consistent with the results from the power spectrum analysis (§ 3); the slope of the Mrk 421 power spectrum is $\alpha \sim 2.1$, and there is a knee frequency at $\sim 4 \times 10^{-6}$ Hz, below which the spectrum flattens; in fact we found that it is highly unlikely that this knee frequency will be smaller than 10^{-7} Hz.

5. DISCUSSION

5.1. *Summary of Results*

All the *EUVE* light curves of Mrk 421 show significant variations (Figs. 4–8). One interpretation is that they are the result of the superposition of flares whose duration, roughly estimated from the same figures, is about 3 days; as an example we quote the 1994 light curve (Fig. 4), where the source flux declines for about 3 days, rises for another ~ 3.5 days, and then stays steady to the end of the observation (~ 3.5 days). We investigated the variability present in the light curves by means of a power spectrum analysis and our results are as follows:

1. On average, the *EUVE* power spectrum of Mrk 421 has a power-law form with a slope $\alpha = 2.14 \pm 0.28$.

2. There is a low-frequency turnover at 4×10^{-6} Hz (i.e., ~ 3 days, the 68% confidence range is 7×10^{-7} Hz to 8×10^{-6} Hz). We cannot determine the shape of the power spectrum below this turnover, nevertheless the data so far is consistent with a flattening of the power spectrum below this frequency to a slope of zero.

3. There is a strong indication that the power spectrum does not remain the same, i.e., that the *EUVE* emission of Mrk 421 is not stationary. The DS 1996 observation shows a power spectrum with a slope $\alpha = 1.1 \pm 0.2$, which is much flatter than the average slope. However, this observation is again consistent with a flattening below the same frequency of 4×10^{-6} Hz.

Furthermore, we performed a structure function analysis of the total *EUVE* light curve. The structure function of the source flattens at timescales greater than 10^6 s. Based on numerical simulations, we found that the Mrk 421 SF is entirely consistent with a 2.14 power spectrum, which flattens to a slope of zero below 4×10^{-6} Hz.

We will discuss each of these results in more detail in the following subsections.

5.2. *The Power Spectrum Slope*

Our analysis shows that, on average, the *EUVE* power spectrum of Mrk 421 (up to $\sim 10^{-4.5}$ Hz) has a power-law form with a slope of $\alpha = 2.14 \pm 0.28$. No periodicities or quasi-periodicities could be found. To the best of our knowledge, this is the first time that the power spectrum of a radio-loud AGN has been estimated in the EUV. In fact, even in the X-rays, the power spectra of radio-loud objects are not well known. The only exception is PKS 2155-304. Its X-ray power spectrum has been estimated in the past (Tagliaferri et al 1991; Zhang et al 1999) to have a slope of ~ -2, similar to the slope of the *EUVE* power spectrum of Mrk 421. Both objects are high-frequency peaked BL Lac objects, and their *EUVE* and X-ray emission are thought to be due to synchrotron radiation. The similarity in the power spectrum slopes could imply that in addition to the same emission mechanism, the same variability mechanism operates in both objects in the two bands.[7]

In general, red noise power spectra can result from a shot-noise model, i.e., from a superposition of random "flare"-like events, each one with the same duration and shape, and with an amplitude randomly distributed around a mean value. A slope $\alpha = 2$ is expected in the case of exponentially decaying shots, consistent with our best-fit slope value. However, the shape of the flares in the *EUVE* light curves of Mrk 421 can by eye, be more complicated than that; they are asymmetric and they do not have the same shape all the times. For example, the first flare in the DS 1995 light curve (Fig. 6) shows a relatively slow rise (it reaches maximum after ~ 2 days), and faster decline (~ 1 day). Immediately after this the source rises again, reaching now the maximum after ~ 1 day. Even if it is not clear what happens after the maximum (if there is a second flare or not), this difference in rise times indicates that the flares are not always the same. Probably, there are flares which rise slow and decay fast and flares with the opposite behavior, or the complicated shapes can be the result of the superposition of consecutive flares.

In general, knowledge of the power spectrum slope alone cannot provide us with much information on the variability mechanism that operates in the source. One has to work the

[7] The normalized amplitude of the PKS 2155-304 X-ray power spectrum at 10^{-5} Hz is greater than 1000 (Zhang et al. 1999), when for Mrk 421 the normalized amplitude of *EUVE* power spectrum at the same frequency, is 148 ± 33 (Table 2).

other way around; develop a model for the variability mechanism, predict the shape of flares, hence the power spectrum slope, and then compare it with the data.

Even though more work is needed in order to investigate if any model can produce light curves with the correct power spectrum slope, amplitude, and low-frequency knee, it is interesting to notice the similarity between the shape of some of the flares in the *EUVE* light curves of Mrk 421 and those predicted by Celotti, Maraschi, & Treves (1991). The flare at the beginning of the DS 1995 light curve (Fig. 6) resemble by eye the flare expected in the case of a perturbation with growing thickness in an inhomogeneous jet (Fig. 4*b* of Celotti et al. 1991). A different behavior is present in the second flare in the same light curve; this time the flux of the source continues to be large after reaching the maximum and the amplitude of the event is smaller than in the previous case. This flare could correspond to the case in Figure 4*a* of Celotti et al. (1991), in which they used different parameters for the stationary jet structure.

5.3. *The Low-Frequency Turnover*

The presence of a low-frequency knee, with a value that remains constant, within the error bars, in all the *EUVE* power spectra of Mrk 421, indicates the presence of a "characteristic timescale" ($t_{\rm var}$) in the system. This timescale determines the "memory" of the system, i.e., the variability mechanism operates in such a way so that, whatever the origin and nature of variations, they "last" typically for a period which is, on average, equal to $t_{\rm var} \sim 1/(4 \times 10^{-6})$Hz ~ 3 days. For example, according to the simple shot noise model mentioned above, the "memory" of the system is determined by the duration of the flares. If, on average, they last for $t_{\rm var}$ days, a low-frequency knee at $\sim 1/t_{\rm var}$ is expected. As we mentioned in the beginning of this section, visual inspection of the Mrk 421 *EUVE* light curves suggests that the flares in them last for ~ 3 days.

The fact that the low-frequency knee remains constant implies that $t_{\rm var}$ is determined by a characteristic of the source that does not change with time. Such a permanent characteristic might be the size of the EUV-emitting region. If that is the case, then an upper limit to the source size at rest frame, R, is given by $R = t_{\rm var} \times (\delta c)$, where δ is the Doppler factor. For $t_{\rm var} \sim 3$ days and a typical value of $\delta \sim 10$, the source size should be less than $\sim 8 \times 10^{16}$ cm. This value is similar to the value of 4.8×10^{16} cm and 4.7×10^{16} cm that Chiaberge & Ghisellini (1999) and Mastichiadis & Kirk (1997) find from theoretical modeling of multifrequency energy spectra of Mrk 421.

Recently, Maraschi et al. (1999) proposed the *e*-folding timescales of 10.7×10^4 s, 7.1×10^4 s, and 5.3×10^4 s at 1, 5, and 15 keV, respectively, for a large flare observed by *BeppoSAX*. These timescales were calculated from a simple arbitrary exponential fitting to a single event in the *BeppoSAX* light curve. If they represent indeed a characteristic timescale of the system at these energies, then this timescale decreases with energy. The timescale derived from EUV data is 2.6×10^5, i.e., larger than the timescales in the X-ray band. If the timescale is associated with the source size, then these numbers are consistent with models in which the source size is expected to decrease with energy. A more detailed comparison has to wait for a proper statistical analysis of the X-ray data.

An indication of a break at ~ 0.5 days is present also in the structure function analysis performed on *BeppoSAX* 2000 observation of Mrk 421 (Y. H. Zhang 2000, private communication). Assuming that the bulk of *BeppoSAX* emission is at ~ 3–4 keV, the 6 times longer EUV (~ 0.1 keV) break could be explained with the synchrotron cooling of the same electron population emitting in the *BeppoSAX* range. The cooling time in fact is proportional to energy of the electrons which emit at a frequency proportional to the inverse of square root of the electron energy. Therefore the cooling time is proportional to the inverse of the square root of the observed frequency.

5.4. *Evidence of Nonstationarity: DS 1996 Data*

As is evident from Figures 9 and 12, the slope of DS 1996 power spectrum (*open circles*) is flatter than the others, showing the nonstationary nature of Mrk 421 emission. The appearance of the DS 1996 light curve (§ 2.2.4) agrees well with the power spectrum of that light curve. The flatter slope of the DS 1996 power spectrum indicates larger amplitude variations at high frequencies, i.e., lots of short time variations, consistent with the presence of a number of short lived flares, and the absence of any long "trend" in the light curve itself. Changes in the power spectrum indicates that some of the variability mechanism characteristics change with time. PKS 2155-304 also shows evidence for nonstationarity in its X-ray light curves (Zhang et al. 1999). Mrk 421 has shown evidence of "nonstationarity" in the past: Fossati et al (2000), in a simultaneous TeV and X-ray observation, found that the hard X-rays were delayed with respect to the soft X-rays, opposite to the behavior previously observed (Takahashi et al 1996).

In the context of the shot-noise model, in DS 1996 power spectrum (1) the different slope indicates a difference in the flare shape, (2) the roughly similar amplitude (Fig. 9) suggests that probably both the number of flares per unit time and their amplitude has not changed drastically during DS 1996 observation, and (3) the knee at the same frequency, within the errors, of the other power spectra indicates that the duration of DS 1996 flares is not changed.

To the eye, though the flares in the DS 1996 light curve appear to be relatively short-lived. We speculate that the DS 1996 flares consist of two parts: one with a fast decay/rise evolution, and another one with a much slower evolution, not seen directly in the light curve, owing to the blending of consecutive flares.

6. CONCLUSIONS

The extremely large *EUVE* database on Mrk 421 (~ 1100 ks) offers a so-far unique opportunity to study the variability properties of a BL Lacertae object at high energies. We analyzed Mrk 421 light curves by means of the power spectrum and structure function techniques; in a power spectrum with slope $\alpha = 2.14 \pm 0.28$ we find indication, confirmed by the structure function analysis, of a break at ~ 3 days. This is the first time that a break in the power spectrum of a BL Lacertae object is found. We also find evidence of nonstationarity for Mrk 421 EUV emission.

The few existing models on BL Lacertae object variability (Celotti et al. 1991; Chiaberge & Ghisellini 1999; Georganopoulos & Marscher 1998), developed for multifrequency analysis, try to explain the amplitude and delays observed among the various energy bands. The single-energy approach, as the one proposed in this paper, is at least as promising as the multifrequency approach, but no predictions on the power spectrum and on the structure

function shapes (the most widely used analysis methods to quantify the variability of an object) have ever been derived from any of the current models.

It is beyond the scope of this paper to investigate in detail whether the model flares that have been computed so far can reproduce the results from the analysis of the *EUVE* light curves of Mrk 421, and we reserve this for a future paper. However, such a quantitative work, will be very interesting since it may be able to distinguish between different models that have been proposed to explain the high-frequency emission of blazars.

We would like to thank A. Celotti, M. Elvis, H. Marshall, and L. Maraschi for useful discussions. We thank the *EUVE* science team and in particular Roger Malina for their logistical support for our continuing analysis effort on *EUVE* data. This research has made extensive use of the High Energy Astrophysics Science Archive Research Center Online Service (HEASARC), provided by the NASA-Goddard Space Flight Center, of the NASA/IPAC Extragalactic Database (NED) operated by the Jet Propulsion Laboratory, Caltech, under contract with NASA and of NASA's Astrophysics Data System Abstract Service. This work was supported by AXAF Science Center NASA contract NAS 8-39073 and by NASA grants NAG 5-3174 and NAG 5-3191. Finally, I. C. thanks the little Ginevra Biaggi for the 4 months long maternity leave during which the bulk of this paper was written.

REFERENCES

Bevington, P. R. 1969, Data Reduction and Error Analysis for the Physical Sciences (New York: McGraw-Hill)
Buckley, J. H., et al. 1996, ApJ, 472, 9
Cagnoni, I., & Fruscione, A. 2000, ApJ, 546, 877 (Paper I)
Celotti, A., Maraschi, L., & Treves, A. 1991, ApJ, 377, 403
Chatfield, C. 1989, The Analysis of Time Series: an Introduction (New York: Chapman and Hall)
Chiaberge, M., & Ghisellini, G. 1999, MNRAS, 306, 551
Deeming, T. J. 1975, Ap&SS, 36, 137
Elvis, M., Wilkes, B. J., & Lockman, F. J. 1989, AJ, 97, 777
Fossati, G., et al. 2000, ApJ, 541, 153
Fruscione, A., Bruhweiler, F., Cheng, K. P., Hall, C. R., Kafatos, M., Ramos, E. & Kondo, Y. 1996, in UV and X-ray Spectroscopy of Astrophysical and Laboratory Plasmas, ed. K. Yamashita & T. Watanabe (Tokyo: Universal Academic), 351
Georganopoulos, M., & Marscher, A. P. 1998, ApJ, 506, 621
Ghisellini, G., Maraschi, L., & Treves, A. 1985, A&A, 146, 204
Kartje, J. F., Konigl, A., Hwang, C. Y., & Bowyer, S. 1997, ApJ, 474, 630
Maraschi, L., et al. 1999, ApJ, 526, L81
Mastichiadis, A., & Kirk, J. G. 1997, A&A, 320, 19
Papadakis, I. E., & Lawrence, A. 1993, MNRAS, 261, 612
———. 1995, MNRAS, 272, 161
Simonetti, J. H., Cordes, J. M., & Heeschen, D. S. 1985, ApJ, 296, 46
Sirk, M.M. 1994, internal EUVE memo MMS/EUVE/0084/94
Tagliaferri, G., Stella, L., Maraschi, L., Treves, A., & Celotti, A. 1991, ApJ, 380, 78
Takahashi, T., et al. 1996, ApJ, 470, 89
Urry, M. C., & Padovani, P. 1995, PASP, 108, 803
Welsh, B. Y., Vallerga, J. V., Jelinsky, P., Vedder, P. W., Bowyer, S., & Malina, R. F. 1990, Opt. Eng., 29, 752
Zhang, Y. H., et al. 1999, ApJ, 527, 719
Zweerink, J. A., et al. 1997, ApJ, 490, 141